

# VERTICAL TEST RESULTS ON KEK-ERL 9-CELL L-BAND SUPERCONDUCTING CAVITY

Enrico Cenni<sup>#</sup>, The Graduate University for Advanced Studies, KEK, Tsukuba, Ibaraki, Japan  
 Takaaki Furuya, Hiroshi Sakai, Kensei Umemori, KEK, Tsukuba, Ibaraki, Japan  
 Kenji Shinoe, ISSP, University of Tokyo, Kashiwa, Chiba, Japan  
 Masaru Sawamura, JAEA, Tokai, Naka, Ibaraki, Japan

## Abstract

In order to develop the Energy Recovery Linac at KEK, we are studying the performance of two prototype L-band superconducting cavities by means of vertical tests. After annealing, electro polishing, high pressure rinsing and baking, several vertical tests were performed and the cavities were inspected through rotating X-ray and temperature mapping system. The performance limiting factor was found to be the field emissions. We observed X-ray emission and temperature raise along the cavity wall. The quench locations were determined with a good agreement between X-ray and temperature sensors. During vertical test we experienced some interesting phenomena such as quality factor degradation and X-ray burst. In the first case the degradation was observed even at low field, however we recovered it with a warming up to room temperature without additional surface treatment. In the latter case new emitters suddenly appeared after some quenches. They remained in the same location also after the warming up. The cavities fulfilled the requirement for the KEK-ERL main linac reaching an accelerating field of more than 20 MV/m.

## INTRODUCTION

Developing and characterization of superconductive cavities is one of the most demanding aspects for the development of a new light source based on Energy Recovery Linac (ERL) concept. At KEK a compact ERL (cERL) is now under construction, to demonstrate the performance of components under CW operation at 100 mA of currents, 3GeV of energy and with ultra-short pulses of 100 fs. Figure 1 shows compact ERL conceptual design.

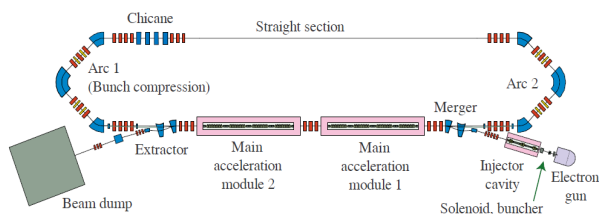


Figure 1: cERL conceptual design

Our group has developed and characterized the superconductive cavities for the main accelerator section.

The performance of two L-band superconductive cavities was studied by means of vertical tests after different surface treatment. In order to obtain a precise diagnosis of the cavities during the tests we have used a rotating mapping system equipped with X-ray and temperature sensors.

## CAVITIES AND EXPERIMENTAL SETUP

Two 1.3GHz superconductive cavities have been manufactured following the design for the main acceleration section of the ERL project. The main parameters for the cavity are summarized in table 1.

One of these cavities was inspected also from a manufacturing point of view. The same model will be installed in cERL so it shall fulfill the high pressure vessel Japanese law, stiffen rings are welded between the center cells while end cells are thicker (3.5mm instead 2.8mm). Moreover titanium end plates were welded between the beam pipes and the end cells, the welding process is also important. Figure 2 shows a detailed view of stiffen rings and titanium end plate.



Figure 2: Detailed view of main acceleration cavities, input port and eccentric fluted beam pipe (left) stiffen rings (right).

Table 1: Parameters of KEK-ERL 9cell cavity

Cavity parameters	
Frequency	1300 MHz
Rsh/Q	897 $\Omega$
Ep/Eacc	3.0
Coupling	3.8%
Q <sub>0</sub> xRs	289 $\Omega$
Hp/Eacc	42.5Oe/(MV/m)

The experimental setup was designed to get X-ray and temperature data from the 9-cell cavity during the vertical test. An array of X-ray sensors (PIN diode) and temperature sensors (carbon resistor) are mounted along the cavity external surface on a rotating stand as shown in figure 3 and figure 4. A total of 82 PIN diodes and 93 carbon resistors are used to detect X-ray produced by field emitted electrons striking the inner surface and heat spots. More detailed description is given in reference [1].

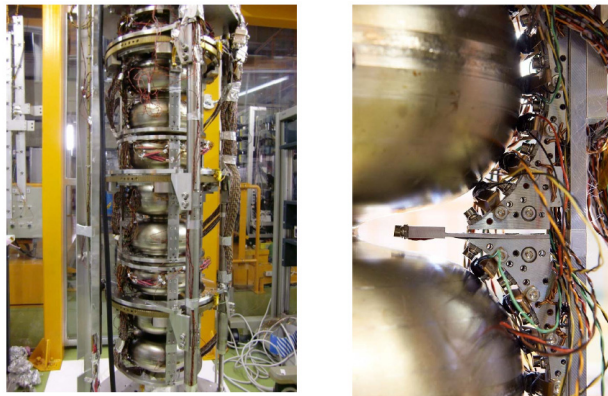


Figure 3: Rotating mapping system for KEK-ERL 9cell cavities

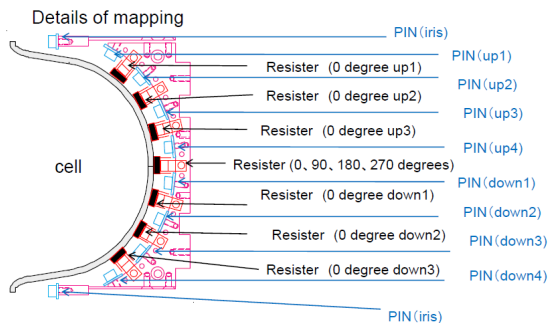


Figure 4: Design detail of the rotating mapping system

### FIRST CAVITY RESULTS

The first cavity results up to the 8<sup>th</sup> vertical tests are detailed in previous papers [2,3], here is just a brief summary of the main features emerged during the tests.

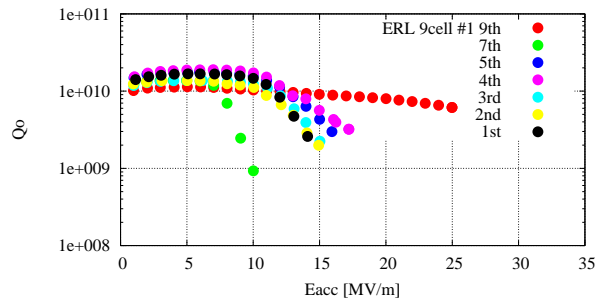


Figure 5: Q<sub>0</sub>-E graph of cavity number 1, from vertical test 1 to 9.

During the vertical tests of the first cavity the main limiting factor to reach higher accelerating field was the field emission. Figure 5 shows the Q-E plot for all the vertical tests performed with the first cavity. Due to the field emission current we also experienced two vacuum leak caused by striking electrons. In the 7<sup>th</sup> test we experienced an X-ray burst, characterized by a quality factor drop as shown in the top part of figure 6 and a sudden appearance of many X-ray traces detected by the mapping system, as shown in bottom part of figure 6.

During the first five tests, copper plated flanges were employed. But in order to avoid problems coming from materials sputtered by field emitted electrons we employed, from the 6<sup>th</sup> test, stainless steel flanges. These flanges had a bigger residual resistance at cryogenic temperature with respect to the copper plated one. This fact led to a quality factor reduction, but meanwhile we could avoid nickel and copper sputtered on the inner surface of the cavity.

The 9<sup>th</sup> vertical test was done after 20  $\mu$ m of electro polishing, high pressure rinsing and a careful assembly in more clean condition. Finally this first cavity achieved an accelerating field of 25MV/m, fulfilling the ERL specification (20MV/m).

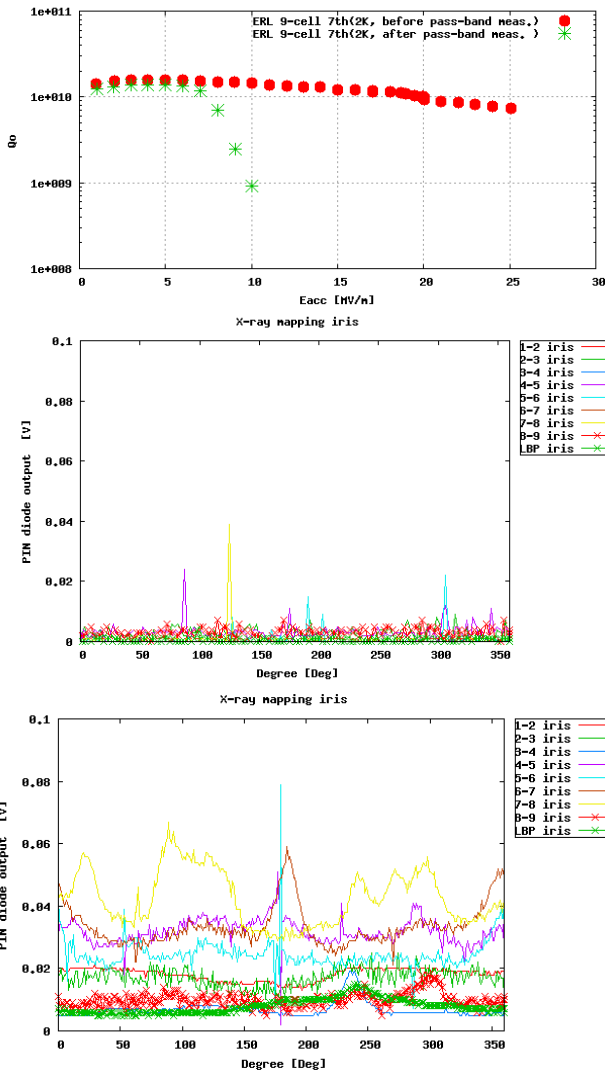


Figure 6: X-ray burst during the 7<sup>th</sup> vertical test of first cavity. Quality factor drop (top) for  $\pi$ -mode: before burst (red dots) and after burst (green dots); Measured X-ray signals set on the cavity iris (middle and bottom), in which x-axis is the angle location around the cavity surface while y-axis is the voltage measured on the PIN diodes (before and after X-ray burst).

### SECOND CAVITY RESULTS

Three vertical tests were performed on the second cavity. A summary of the treatments with tests results are collected in the table 2. Also obtained Q-E plots are shown in figure 7. During the 3<sup>rd</sup> test second sound sensors were mounted. As for the previous cavity we employed stainless steel flanges, so the total quality factor was reduced with respect to test in which copper plated flanges were used.

Table 2: History of 2<sup>nd</sup> cavity

	Surface treatment	Maximum gradient at final state	Comment
Before vertical tests	Electro Polishing (100 $\mu$ m), Annealing, EP2(20 $\mu$ m), High Pressure Rinsing, Baking		
1 <sup>st</sup>		23MV/m	Field emission, Satisfy ERL requirement
2 <sup>nd</sup>	EP2(20 $\mu$ m), HPR, Baking	24 MV/m	Field emission, Satisfy ERL requirement
3 <sup>rd</sup>	Warm up	24 MV/m	Same as 2 <sup>nd</sup> measure

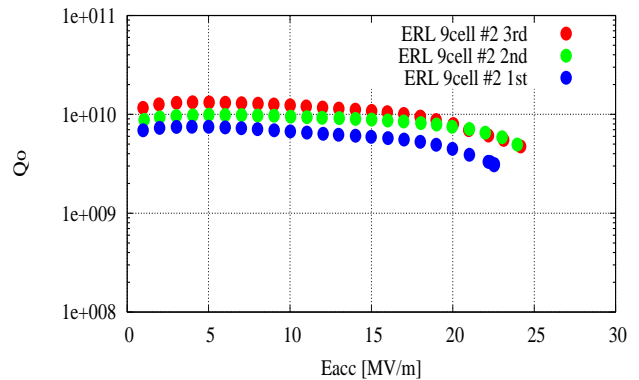


Figure 7: Q<sub>0</sub>-E graph of cavity number 2, from vertical test 1 to 3.

As listed in table 2, all the vertical tests confirmed that the cavity could fulfill the ERL specification. In this phase the limiting factor to reach higher accelerating field was the field emission from the cavity surface.

During these vertical tests, we experienced some interesting phenomena. One was an X-ray burst, which was again occurred at the 2nd vertical test. It caused the drop of Q-values at higher field. Another was gradual decreasing of quality factor, which was observed during processing. Also the quench location was detected, with a good agreement by means of X-ray mapping and temperature mapping. Even temperature profile was measured with respect to the accelerating field until quenches occurred.

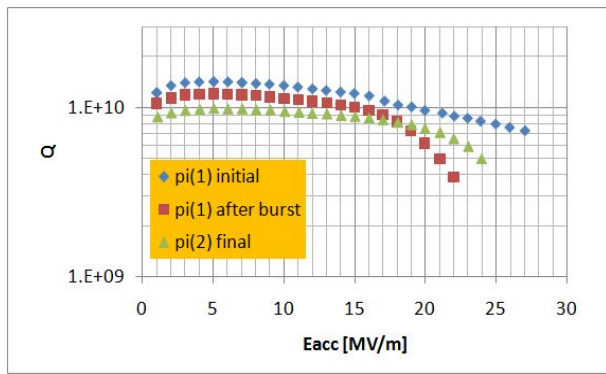


Figure 8: Q-E graph for the 2nd vertical test. Blue points show the initial state. Red ones show after X-ray burst. Green ones show after processing.

In figure 8, it is possible to see the Q-E graph during the second vertical test. The initial state of the cavity was really promising. An accelerating field of 28MV/m was obtained with small field emission (blue curve). Nevertheless at 28MV/m a quench occurred accompanied by many abnormal X-ray signals. After this event, field emission was detected from about 16MV/m (red curve). Also after processing with pass band mode, the cavity quality factor was degraded with respect to the initial one (green curve).

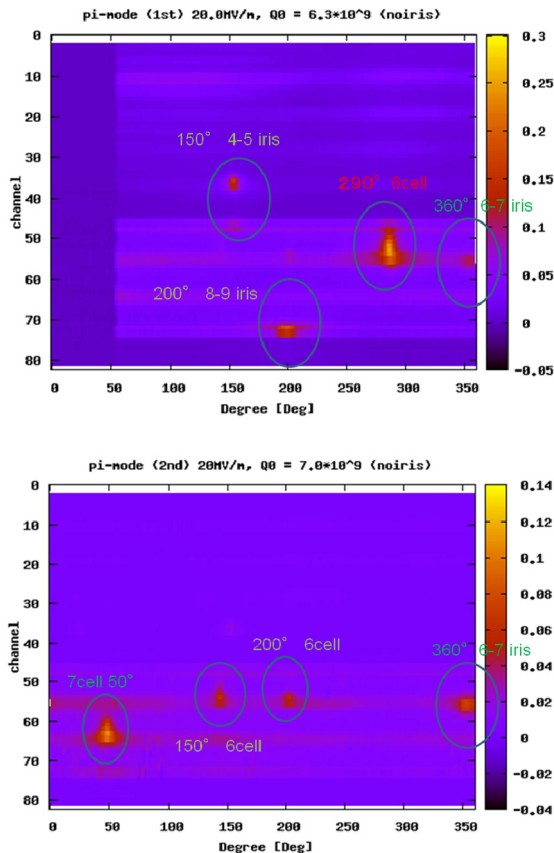


Figure 9: X-mapping during  $\pi$ -mode operation at 20MV/m: after X-ray burst (top), after processing (bottom); x-axis is the angle location around the cavity

surface and y-axis is the location along the cavity length. The 9 cell is located in the bottom part while the 1 cell in the upper.

In the top of figure 9 the X-ray mapping during the second vertical test is shown. The accelerating field was 20MV/m and the quality factor was  $6.3 \times 10^9$ . The data was obtained after the X-ray burst event, before it X-ray signals were almost negligible. As shown in the top part of figure 9, four emitters were clearly visible, they were located at 150°, 200°, 290° and 360°. The detected X-ray signals were respectively located around the 4-5 cell iris, 8-9 cell iris, along the 6 cell and on the 6-7 cell iris. After the  $\pi$ -mode operation was performed, pass band modes were measured. Some emitters were processed during this operation but some new appeared. In the bottom part of figure 9, the X-ray mapping was shown during  $\pi$ -mode operation after the processing phase. The accelerating field was 20MV/m and the quality factor was  $7.0 \times 10^9$ . The emitters located at 200° and 290° seemed to be processed during the pass band mode operation, while some new emitters appeared mainly around the sixth cell. With reference to figure 8, the two mapping images shown in figure 9 represent the cavity status at 20MV/m after the burst (red curve) and at the same accelerating field after the processing (green curve).

As shown in figure 7 or 8, a quality factor was degraded during processing at the whole lower accelerating field than 15MV/m.

Magnetic flux trapping or niobium surface damages under processing are considered to be possible reasons of this degradation.

To investigate the source of quality factor degradation, it was decided to warm up the cavity without any other surface treatment before performing a third vertical test.

At the third vertical test the quality factor at lower accelerating field than 15MV/m was successfully recovered as shown in the figure 10.

One possible reason of the quality factor degradation was mainly due to the magnetic field trapping.

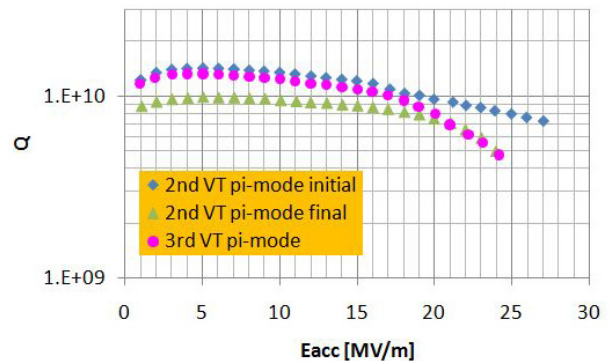


Figure 10: Q-E graph of cavity number 2, 2nd test initial  $\pi$ -mode (blue), 2nd test final  $\pi$ -mode after quench, quality factor curve has an offset (green), 3rd test  $\pi$ -mode (pink)

Also mapping data was obtained at the same condition with the accelerating field of 20MV/m as shown in figure 11, at the 3rd vertical test.

Many X-ray traces are still present. Comparing with the bottom of figure 9, almost all are shown at the same location.

These results indicate that the source of emitters, which produced X-ray traces, was not due to gas absorption. In this case, warming-up did not help to reduce field emissions.

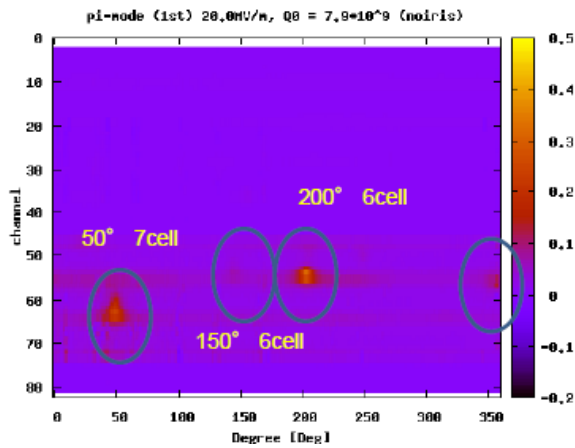


Figure 11: X-ray mapping during initial  $\pi$ -mode operation at 20MV/m (third vertical test). x-axis is the angle location around the cavity surface and y-axis is the location along the cavity length. The 9 cell is located in the bottom part while the 1 cell in the upper.

At the 3rd vertical test, temperature data were collected more precisely than before. Until this test collecting this data was difficult due to the low signal to noise ratio during the movement of the rotating mapping system. Figure 12 shows the mapping data taken during  $\pi$ -mode operation with an accelerating field of 23MV/m. The top part of the figure 12 shows the X-ray data while the bottom part the temperature measured data. The data show a clear peak located around the bottom part of the 7 cell at 50° angle. As a consequence of this measurement, we moved the temperature sensors near the quenching spot exploiting the flexibility of the rotating mapping system.

In fact to investigate with more details, sensors were fixed to 50°, where both temperature and X-ray traces were observed. During this test second sound sensors were also mounted, but without a precise calibration, nevertheless also the second sound data show a quench spot in the same location of X-ray and temperature sensors.

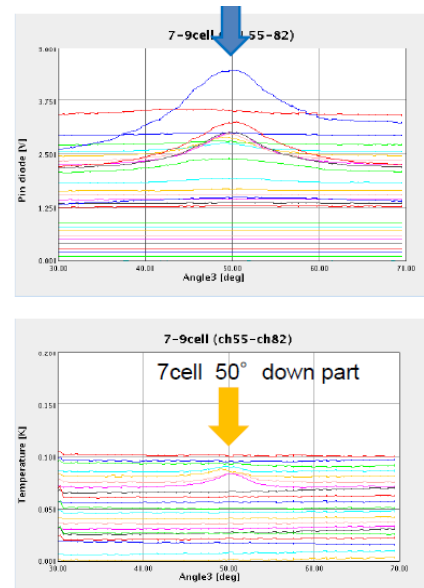


Figure 12: X-mapping (top) and T-mapping (bottom) at the field of 23 MV/m. The spot is located at 50° in the 7<sup>th</sup> cell down part.

Figure 13 shows the data collected with temperature sensors placed near the quench location. X-axis of this graph shows the accelerating field magnitude (MV/m) while on y-axis the temperature change between the sensor and the He bath temperature (K). As shown previously in figure 12 a small temperature rise was detected, a clear signal of temperature rise from 23MV/m was observed. When the accelerating field was risen up to 25MV/m and quench was occurred. The temperature increase was about 5K. From this characteristics, it seems that the quench was generated by field emission electrons.

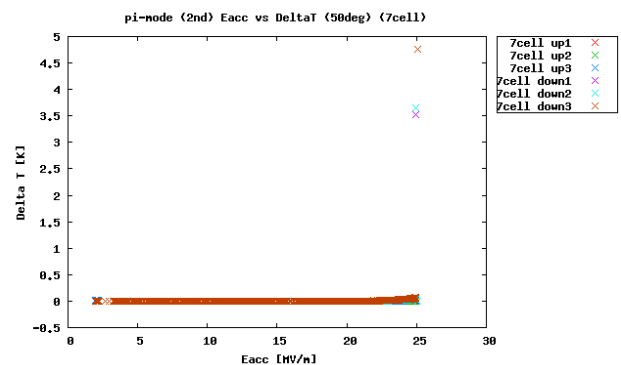


Figure 13: Temperature change between the sensor and the He bath temperature in the proximity of the quench location

### SUMMARY

Two cavities for the main acceleration section of cERL were tested and characterized by means of vertical tests. The peculiar phenomena concerning field emitted electrons was analyzed with temperature and X-ray rotating mapping system. During a vertical test we experienced a sudden X-ray burst that led to the

appearance of new emitters along the inner surface of the cavity. Another phenomenon, experienced during processing, was the quality factor degradation. Nevertheless after a warming-up, the quality factor was recovered, but the emitters were still present. They were clearly visible as X-ray traces. These cavities achieved more than 20 MV/m and satisfied the requirement for ERL main linac.

### REFERENCES

- [1] H. Sakai, et al., Proc. of IPAC10, p. 2950.
- [2] K. Umemori, et al., Proc. of SRF2009, p. 896.
- [3] K. Umemori, et al., Proc. of IPAC10, p. 2956.